Memory function of turbulent fluctuations in soft-mode turbulence

Takayuki Narumi,[1,*] Junichi Yoshitani,[1] Masaru Suzuki,[1] Yoshiki Hidaka,[1,†] Fahrudin Nugroho,[1,2]
Tomoyuki Nagaya,[3] and Shoichi Kai[1]

[1]*Department of Applied Quantum Physics and Nuclear Engineering, Kyushu University, Fukuoka 819-0395, Japan*
[2]*Physics Department, Gadjah Mada University, Yogyakarta 55281, Indonesia*
[3]*Department of Electrical and Electronic Engineering, Oita University, Oita 870-1192, Japan*
(Received 31 October 2012; revised manuscript received 25 December 2012; published 23 January 2013)

Modal relaxation dynamics has been observed experimentally to clarify statistical-physical properties of soft-mode turbulence, the spatiotemporal chaos observed in homeotropically aligned nematic liquid crystals. We found a dual structure, dynamical crossover associated with violation of time-reversal invariance, the corresponding time scales satisfying a dynamical scaling law. To specify the origin of the dual structure, the memory function due to nonthermal fluctuations has been defined by a projection-operator method and obtained numerically using experimental results. The results of the memory function suggest that the nonthermal fluctuations can be divided into Markov and non-Markov contributions; the latter is called the turbulent fluctuation (TF). Consequently, the relaxation dynamics is separated into three characteristic stages: bare-friction, early, and late stages. If the dissipation due to TFs dominates over that of the Markov contribution, the bare-friction stage contracts; the early and late stages then configure the dual structure. The memory effect due to TFs results in a time-reversible relaxation at the early stage, and the disappearance of the memory by turbulent mixing leads to a simple exponential relaxation at the late stage. Furthermore, the memory effect due to TFs is shown to originate from characteristic spatial coherency called the patch structure.

I. INTRODUCTION

Weak nonlinearity can generate spatial and temporal disorders in systems where the number of effective degrees of freedom increases with increasing system size. A phenomenon triggered by weak nonlinearity in such high-dimensional systems is called spatiotemporal chaos, in contrast with chaos where unpredictable behavior emerges from a few degrees of freedom in a deterministic way. Theoretical work on the spatiotemporal chaos (Refs. [1,2], and references therein) has covered topics such as the complex Ginzburg-Landau equation, the Kuramoto-Sivashinsky turbulence (KST), the Nikolaevskii turbulence, and coupled map lattices. An outstanding feature of chaos and turbulence is its dual structure, where the dynamics is separated into an *initial* regime corresponding to deterministic short orbits and a *final* regime corresponding to stochastic long orbits. Mori and Okamura, for example, have theoretically studied one-dimensional (1D) KST and revealed the dual structure in turbulent mixing by numerical analysis [3].

Convection systems have been experimentally investigated to study nonlinearity. An example is electrohydrodynamic convection observed in the nematic liquid crystal and controlled by an ac voltage applied to the system. One can easily achieve accessible characteristic length and time scales in experiments of electroconvection compared with the Rayleigh-Bénard convection. Another advantage of investigating nematics is the ease in controlling the anisotropy to study symmetry properties. There are two types of layer alignment in nematic liquid crystals; one is planar alignment in which the

director aligns parallel to substrates (x direction), and the other is homeotropic alignment in which the director aligns perpendicular to substrates (z direction). Rubbing along the x direction of a substrate's surface (x-y plane) produces planar systems and intrinsically breaks the rotational symmetry. In homeotropic systems, by contrast, the rotational symmetry in the x-y plane remains. With a sufficiently strong applied ac voltage, magnitude V, and fixed frequency f, the Fréedericksz transition, occurring at a certain threshold voltage V_F, spontaneously breaks the rotational symmetry [4]; the transition is accompanied by the excitation of the Nambu-Goldstone modes [5–7]. By further increasing V, electrohydrodynamic convection occurs at V_c. The nonlinear coupling between the convective and Nambu-Goldstone modes generates a pattern that is both spatially and temporally disordered. The experimentally observed phenomenon, called soft-mode turbulence (SMT), is an example of spatiotemporal chaos [8–10].

In our preceding study, we observed SMT relaxation by measuring a temporal autocorrelation function and reported that the relaxation is well fitted by a compressed exponential function [11]. Because the compressed exponential is employed to describe the dynamics of jammed systems [12], we remarked on the similarity between SMT and glass forming liquids. The nonlinearity in the dynamics of the latter originates from dynamic coherency in some regions. In fact, spatiotemporal fluctuating cooperative regions have been observed as dynamical heterogeneities near the glass transition point [13–16]. A characteristic length for these cooperative regions increases as the glass transition point is approached. In SMT, on the other hand, patch domains exist in which convective rolls align in a unique orientation [17–19]. The characteristic size ξ of a patch domain is several times longer than the typical size of convective rolls and decreases with the distance from SMT onset; $\xi \sim \varepsilon^{-1/2}$ with

*narumi@athena.ap.kyushu-u.ac.jp
†hidaka@ap.kyushu-u.ac.jp

control parameter ε. We have therefore concluded that the SMT patch domains behave like the cooperative regions in glass forming liquids and the coherent motion in the domains generates nonexponential relaxation. To study SMT dynamics in detail, the temporal correlations of each wave number, *modal* autocorrelation functions, are suitable. Our previous study focused on the *net* autocorrelation function consisting of the entire wave-number information. Here, we investigate the modal relaxation dynamics to specify the statistical physics of SMT.

II. EXPERIMENT

We study the two-dimensional pattern dynamics of SMT observed in a homeotropic alignment of nematic liquid crystals. This study follows a standard setup [8,20,21]. The space between two parallel glass plates, spaced 27 μm apart, was filled with a nematic liquid crystal, *N*-(4-methoxybenzilidene)-4-buthylaniline. The plate surfaces were coated with transparent electrodes, made of indium tin oxide with a circular cross section of radius 13 mm. To obtain homeotropic alignment, the surfaces were covered by a surfactant, N,N-dimethyl-N-octadecyl-3-aminopropyl-trimethoxysilyl chloride 50%. The values of the dielectric constant and electric conductivity parallel to the director were $\epsilon_\parallel = 6.25$ and $\sigma_\parallel = 1.17 \times 10^{-7}\ \Omega^{-1}\ \mathrm{m}^{-1}$, respectively. Denoting the dielectric constant perpendicular to the director by $\epsilon_\perp$, the dielectric constant anisotropy $\epsilon_a = \epsilon_\parallel - \epsilon_\perp$ is found to be negative. An ac voltage, $V(t) = \sqrt{2}V\cos(2\pi f t)$, was applied to the sample. For a control parameter, we employed a normalized voltage, $\varepsilon = (V/V_\mathrm{c})^2 - 1$, where V_c denotes the threshold voltage for electroconvection having a value of 7.78 ± 0.05 V. We show results for $\varepsilon = 0.025, 0.050, 0.075, 0.10, 0.20, 0.30$, and 0.40, where ε has a margin of error of ± 0.013. Another control parameter was the frequency f of the ac voltage. Two patterns of SMT arise: oblique roll in $f < f_\mathrm{L}$ and normal roll in $f > f_\mathrm{L}$, where f_L denotes the Lifshitz frequency [8,9]. We set the frequency $f = 100\,\mathrm{Hz}$ well below f_L. The temperature was regulated to $30.00 \pm 0.05\,^\circ$C. Before each sampling, we waited for 10 min at the fixed voltage V_w and then a further 10 min at the set V to get a desired ε value, where $V_\mathrm{F} < V_\mathrm{w} < V_\mathrm{c}$. The waiting time was sufficiently long for systems to achieve steady state.

The electroconvection pattern was observed by a microscope (ECLIPSE E600POL, Nikon Corporation, Tokyo) and was captured by a high-speed camera (HAS220, DITECT Co., Ltd., Tokyo) that can successively take 4200 frames. The numbers of frames per second were 5 for $\varepsilon < 0.1$ and 10 otherwise. A typical two-dimensional image is shown in Fig. 1(a). The measurement area was $830 \times 830\ \mu$m^2 (450×450 pixels). The transmitted light intensity $I(\boldsymbol{x},t)$ at each pixel was digitized into 8-bit (i.e., 256-level) information, where a series of pattern analyzing was processed according to Ref. [22].

With angle brackets signifying the long-time average in the steady state, the temporal correlation of two functions is defined as

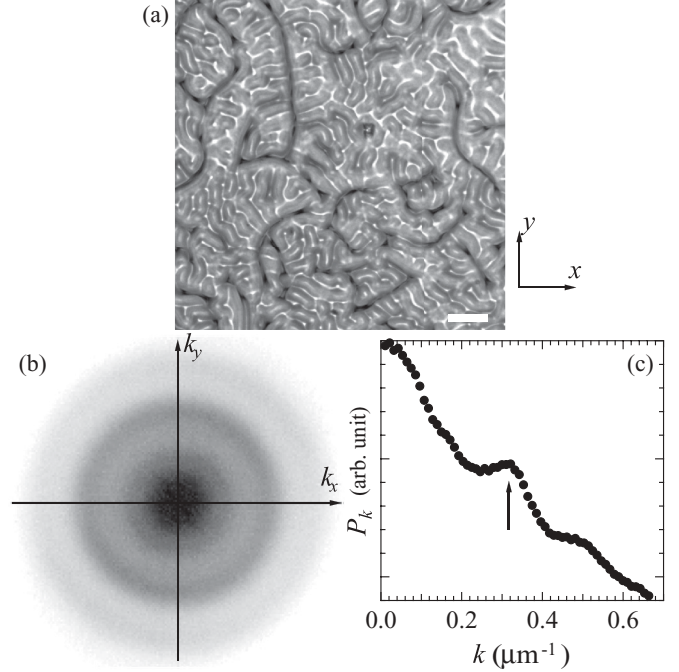$$\langle f(t+\tau)g(t)\rangle = \lim_{T\to\infty}\frac{1}{2T}\int_{-T}^{T}dt\,f(t+\tau)g(t). \quad (1)$$

FIG. 1. Static information of our experiment at $\varepsilon = 0.10$. (a) A typical snapshot of SMT with the white scale bar indicating 100 μm. Each bright line indicates upward flow. (b) Magnitude tints of the spatial power spectrum P_k in the Fourier space, where shading corresponds to the P_k value. (c) Plot of the power spectrum P_k as a function of the radial wave number $k = |\boldsymbol{k}|$. The peak, marked by an arrow, corresponds to the fundamental period in a convective rolling.

We employ the Fourier transform of the fluctuation $\Delta I(\boldsymbol{x},t) = I(\boldsymbol{x},t) - \langle I(\boldsymbol{x},t)\rangle$ as the gross variable $u_{\boldsymbol{k}}(t)$:

$$u_{\boldsymbol{k}}(t) := \int d\boldsymbol{x}\,\Delta I(\boldsymbol{x},t)e^{i\boldsymbol{k}\cdot\boldsymbol{x}}, \quad (2)$$

where $i = \sqrt{-1}$ and the integral range is over the entire system domain. In isotropic systems, it is sufficient to study $u_k(t)$ [23], where k denotes the radial wave number, $k = |\boldsymbol{k}|$. We focus on the normalized modal time-correlation function of k:

$$\hat{U}_k(\tau) := \langle u_k(t+\tau)u_k^*(t)\rangle P_k^{-1}, \quad (3)$$

where the asterisk denotes the complex conjugate operation and $P_k = \langle|u_k(t)|^2\rangle$ denotes the spatial power spectrum. Note that $\hat{U}_k(\tau)$ is a real number due to translational symmetry and isotropy. The spatial power spectra as functions of the wave number $\boldsymbol{k}$ and $k = |\boldsymbol{k}|$ are illustrated in Fig. 1(b) and 1(c), respectively. SMT isotropy is clearly reflected in Fig. 1(b). Although the experimental parameters in Ref. [23] are slightly different from ours, the P_k profiles agree. A clear peak exists at $k_\mathrm{peak} \simeq 0.321\ \mu$m^{-1} for $\varepsilon = 0.10$ and its corresponding length $\lambda_\mathrm{peak} = 2\pi/k_\mathrm{peak}$ is 19.6 μm, which is a half of λ_0, where $\lambda_0 = \lambda_0(\varepsilon)$ denotes the length of a pair of electroconvections. The peak wave numbers k_peak for other ε values are similar. The wave number k is normalized by λ_0 as $\hat{k} = k\lambda_0/2\pi$.
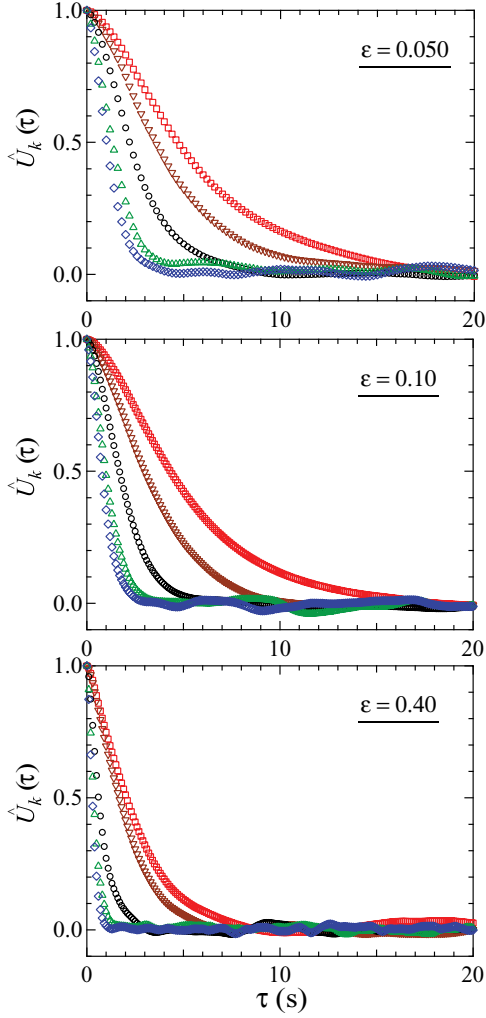
FIG. 2. (Color online) Plot of the modal correlation functions at $\varepsilon = 0.050$ (top), 0.10 (middle), and 0.40 (bottom). The wave numbers, $\hat{k}$, are 0.76 (red square), 1.0 (brown inverted triangle), 2.0 (black circle), 3.0 (green triangle), and 4.0 (blue diamond).

III. RESULTS AND DISCUSSION

A. Dual relaxation

The modal autocorrelation function $\hat{U}_k(t)$ obtained experimentally is shown in Fig. 2. In the short-time regime, the relaxation is not described by a simple exponential function. Instead, we found dual relaxation as evident in Fig. 3. In the early stage [24], the correlation function follows an algebraic decay form:

$$\hat{U}_k(\tau) \propto 1 - \left(\tau / \tau_k^{(a)}\right)^2. \tag{4}$$

In contrast, the relaxation in the late stage is well described by exponential decay:

$$\hat{U}_k(\tau) \propto \exp\left[-\tau / \tau_k^{(e)}\right]. \tag{5}$$

Figure 4 presents the characteristic time scales at each stage for the dual structure. The time scales are almost constant at small wave numbers. Note that the results at small $\hat{k}$ may be affected by limitations in sample averaging. At large wave numbers, the time scales of the dual relaxation satisfy dynamic
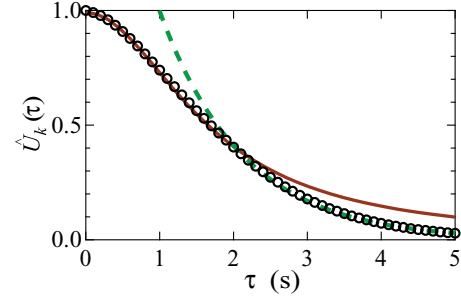

FIG. 3. (Color online) The normalized modal autocorrelation function of $\varepsilon = 0.10$ and $\hat{k} = 2.0$, which is the same as shown in Fig. 2. The algebraic decay (4) (brown solid line) well describes the dynamics in the early stage, but a simple exponential (5) (green dashed line) is better at the late stage.

scaling laws:

$$\tau_k^{(a)} \propto \hat{k}^{-z_a}, \quad \tau_k^{(e)} \propto \hat{k}^{-z_e}, \tag{6}$$

with dynamical exponents $z_a \simeq 1.0$ and $z_e \simeq 1.5$ regardless of ε. Although Mori and Okamura have reported that the dynamical scaling exponents obtained theoretically in 1D KST are $z_a = 1$ and $z_e = 2$ [3], we cannot directly compare our results with their theoretical work because the dynamical exponent depends on spatial dimensionality. Indeed, dynamic scaling for several turbulence models depends on the dimensionality [25–27].

To elucidate the dual structure of SMT theoretically, we have taken into account the experimental fact that the spatiotemporal disorder accompanied by the patch structure can be represented as nonthermal fluctuations [17,28].
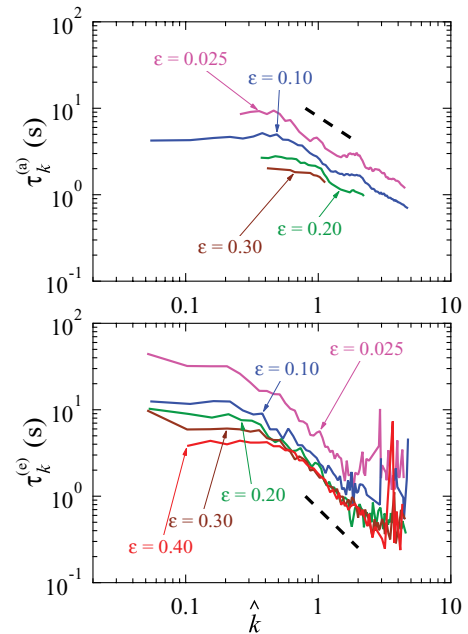

FIG. 4. (Color online) Log-log plots of time scales $\tau_k^{(a)}$ (top) and $\tau_k^{(e)}$ (bottom) for several control parameters: $\varepsilon = 0.025$ (pink), 0.10 (blue), 0.20 (green), 0.30 (brown), and 0.40 (red). The dashed lines plot the power law with exponents $z_a = 1.0$ (top panel) and $z_e = 1.5$ (bottom panel).
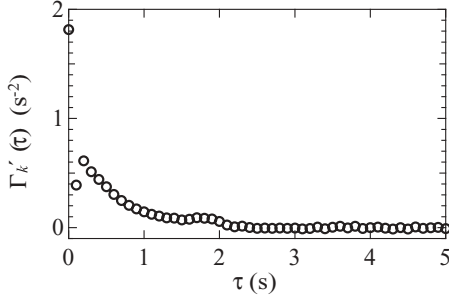
FIG. 5. The memory function $\Gamma'_k(\tau)$ characterized by Eq. (7). This is the result of $\varepsilon = 0.10$ and $\hat{k} = 2.0$ as an example.

The projection-operator method for turbulence [29] is one of the most suitable methods to manage such nonthermal fluctuations; its mathematical procedure derives an evolution equation containing the memory effect that is equivalent to the autocorrelation of fluctuations (see Appendix). Thus, in the rest of the paper, analysis for the memory functions plays a central role in studying the relationship between the dual structure and the nonthermal fluctuations.

B. Memory effect due to nonthermal fluctuations

We assume the modal elements $\{u_k\}$ form a complete set of macroscopic variables in SMT [30]. According to the projection-operator formalism, the evolution equation in SMT is represented as

$$\frac{\partial \hat{U}_k(\tau)}{\partial \tau} = -\int_0^\tau d\tau' \Gamma'_k(\tau - \tau')\hat{U}_k(\tau'), \qquad (7)$$

where $\Gamma'_k(\tau)$ denotes the memory function that results from the nonthermal fluctuations. Here, translational symmetry reduces the temporal correlation of the modal elements to

$$\langle u_k(t+\tau)u^*_{k'}(t)\rangle = \delta_{k,k'}\langle u_k(t+\tau)u^*_k(t)\rangle, \qquad (8)$$

and the mechanical coefficients ω_{kk} are zero by definition.

Using experimental results for the modal correlation function, one can numerically solve Eq. (7) to obtain the memory function. The memory function $\Gamma'_k(\tau)$ has a sharp peak at $\tau = 0$, as evident in Fig. 5, implying that the nonthermal fluctuations can be separated into Markov and non-Markov contributions. Therefore, with

$$\Gamma'_k(\tau) = 2\gamma^{(0)}_k \delta(\tau) + \Gamma_k(\tau), \qquad (9)$$

where $\gamma^{(0)}_k$ denotes the bare friction due to the Markov contribution of the nonthermal fluctuations and $\Gamma_k(\tau)$ the memory function due to the non-Markov contribution, the evolution equation (7) reduces to

$$\frac{\partial \hat{U}_k(\tau)}{\partial \tau} = -\gamma^{(0)}_k \hat{U}_k(\tau) - \int_0^\tau d\tau' \Gamma_k(\tau - \tau')\hat{U}_k(\tau'). \quad (10)$$

To emphasize the transport due to the turbulentlike dynamics, the non-Markov contribution to the nonthermal fluctuations is here called the *turbulent fluctuations* (TFs) in SMT. One can define a characteristic time scale for the memory function due to TFs as

$$\tau^{(\Gamma)}_k := \frac{1}{\Gamma_k(0)}\int_0^\infty d\tau \Gamma_k(\tau), \qquad (11)$$

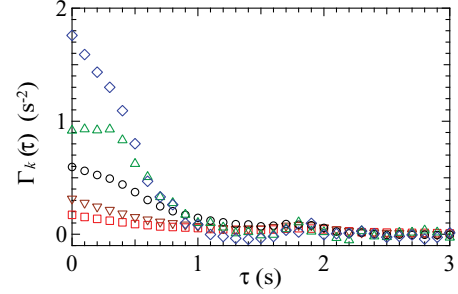within which the memory effects due to TFs are alive.

FIG. 6. (Color online) Time dependence of the memory function for $\varepsilon = 0.10$ at several fixed wave numbers: $\hat{k} = 0.76$ (red square), 1.0 (brown inverted triangle), 2.0 (black circle), 3.0 (green triangle), and 4.0 (blue diamond).

As seen in Fig. 6, the memory function $\Gamma_k(t)$ caused by TFs has non-negligible magnitudes and time scales over a range of wave numbers in the early stage; therefore, SMT dynamics is regarded as being non-Markovian due to TFs. The memory has a small peak around $\tau \simeq 2$ s. We believe that this is due to a residual of the mechanical coefficient appearing in the projection-operator method, despite the coefficient being theoretically zero.

Each equation of the dual relaxation is elucidated by the evolution equation (10). First, let us consider the dynamics at the late stage, $\tau^{(\Gamma)}_k \ll \tau$. The frequency-dependent friction $\Gamma_{k,\omega}$ caused by TFs is defined as the Fourier-Laplace transformation of the memory function:

$$\Gamma_{k,\omega} := \int_0^\infty d\tau \Gamma_k(\tau)e^{i\omega\tau}. \qquad (12)$$

At the late stage, friction can be regarded as static,

$$\gamma^{(\Gamma)}_k := \Gamma_{k,\omega=0}; \qquad (13)$$

hence, the memory effect is approximated by a δ function,

$$\Gamma_k(\tau) \simeq 2\gamma^{(\Gamma)}_k \delta(\tau). \qquad (14)$$

The modal relaxation dynamics is thus obtained as a simple exponential function (5) with the characteristic time:

$$\tau^{(e)}_k = \left(\gamma^{(0)}_k + \gamma^{(\Gamma)}_k\right)^{-1}. \qquad (15)$$

Next, at $\tau \ll \tau^{(\Gamma)}_k$, an approximate solution of Eq. (10) is

$$\hat{U}_k(\tau) = 1 - \frac{\gamma^{(\Gamma)}_k}{\tau^{(\Gamma)}_k}\int_0^\tau d\tau'\left(\tilde{\gamma}_k\tau^{(\Gamma)}_k + \tau'\right) + \mathcal{O}(\tau^3), \qquad (16)$$

with $\tilde{\gamma}_k = \gamma^{(0)}_k/\gamma^{(\Gamma)}_k$. Thus, if $\tilde{\gamma}_k \ll 1$, the time range can be separated into $\tau \ll \tilde{\gamma}_k\tau^{(\Gamma)}_k$ and $\tilde{\gamma}_k\tau^{(\Gamma)}_k \ll \tau \ll \tau^{(\Gamma)}_k$. In the shorter time regime $\tau \ll \tilde{\gamma}_k\tau^{(\Gamma)}_k$, called the bare-friction stage, modal relaxation decays linearly with slope $\gamma^{(0)}_k$. In contrast, it reduces to time-reversible algebraic decay in the longer time regime $\tilde{\gamma}_k\tau^{(\Gamma)}_k \ll \tau \ll \tau^{(\Gamma)}_k$, i.e., the early stage of the dual structure with characteristic time,

$$\tau^{(a)}_k = \sqrt{2\tau^{(\Gamma)}_k/\gamma^{(\Gamma)}_k}. \qquad (17)$$

TABLE I. Characteristic stages of modal relaxation dynamics in soft-mode turbulence.

Stage	Time range	Decay form
Bare-friction stage	$\tau \ll \tilde{\gamma}_k \tau_k^{(\Gamma)}$	Linear decay caused by the Markov fluctuations.
Early stage	$\tilde{\gamma}_k \tau_k^{(\Gamma)} \ll \tau \ll \tau_k^{(\Gamma)}$	Time-reversible decay that originates from memory due to TFs [Eq. (4)].
Late stage	$\tau_k^{(\Gamma)} \ll \tau$	Simple exponential decay after turbulent mixing [Eq. (5)].

Therefore, a small ratio $\tilde{\gamma}_k$ of the friction coefficients is a necessary requirement for the appearance of dual relaxation in SMT. The characteristic stages are summarized in Table I.

C. Characteristic time scales

A characteristic time scale for the modal autocorrelation function can be defined by

$$\tau_k^{(U)} := \int_0^\infty d\tau \, \hat{U}_k(\tau). \tag{18}$$

This is the relaxation time due to nonthermal fluctuations. In contrast, the time scale $1/\gamma_k^{(0)}$ denotes the relaxation time due to Markov fluctuations only. From the evolution equation (10), $\tau_k^{(U)}$ is exactly represented by the friction coefficients,

$$\tau_k^{(U)} = \left(\gamma_k^{(0)} + \gamma_k^{(\Gamma)} \right)^{-1}. \tag{19}$$

Therefore, $\tau_k^{(U)}$ is nearly equal to $\tau_k^{(e)}$ according to Eq. (15); its accuracy has been confirmed within the margins of numerical error, indicating that the approximation (14) is reasonable.

The characteristic time scale $\tau_k^{(\Gamma)}$, plotted as a function of normalized wave number in Fig. 7, has a weak peak in $\hat{k} < 2$ for each ε. Let k_Γ denote the wave number at which $\tau_k^{(\Gamma)}$ has a peak, where k_Γ is determined by a method for multipeak fitting so that roughness of curves is smoothed. In expectation that the coherency in patch domains leads to the non-Markov memory effect, the time scale $\tau_k^{(\Gamma)}$ should include features relating to the patch domains. The length scale $\lambda_\Gamma = 2\pi/k_\Gamma$ is several times larger than the diameter of an electroconvective roll. In addition, the power law $\lambda_\Gamma \propto \varepsilon^{-1/2}$ is quantitatively reasonable as indicated in Fig. 8. Therefore, it follows that the dual relaxation caused by TFs originates from the patch structure. The time scale rapidly decreases at larger length scales, $k < k_\Gamma$, indicating that interpatch dynamics does not affect the memory effect due to TFs. Some work does support
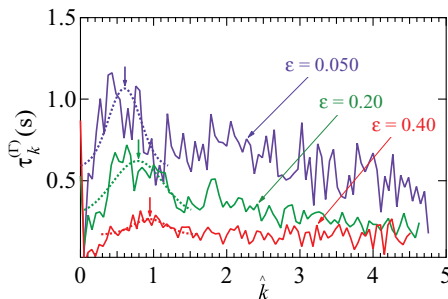
the relationship between the patch structure and the dual structure [17,28,31], where the dynamics of a tagged particle in the SMT disorder can be divided into two types of mode: one dominated by convective rolling within patch domains (i.e., intrapatch dynamics) and the other dominated by transfers with slow patch movements (i.e., interpatch dynamics).

Figure 9 shows corresponding dispersion relations. The friction $\gamma_k^{(\Gamma)}$ is 1 order larger than the bare friction $\gamma_k^{(0)}$ near k_Γ, but converges at large wave numbers. A characteristic feature is a dip appearing near $\hat{k} \simeq 1$ in $\gamma_k^{(0)}$ but not in $\gamma_k^{(\Gamma)}$. The bare friction $\gamma_k^{(0)}$ and the static friction $\gamma_k^{(\Gamma)}$ caused by TFs are explicitly related to the average rate in entropy production $\dot{S}_k$ [29]. Over a macroscopic time scale, it is analytically represented as

$$\dot{S}_k = k_B \left(\gamma_k^{(0)} + \gamma_k^{(\Gamma)} \right) = k_B / \tau_k^{(U)}, \tag{20}$$

where k_B is the Boltzmann constant. The dip might reflect a law of minimum entropy production rate in electroconvection.

The time scales, $\tau_k^{(U)}$, $\tau_k^{(\Gamma)}$, and $\tilde{\gamma}_k \tau_k^{(\Gamma)}$, are compared in Fig. 10 for several ε values. The correlation time $\tau_k^{(U)}$ is much longer than $\tau_k^{(\Gamma)}$ at large length scales, where the relaxation dynamics is approximately represented by a simple exponential. The ratio $\tau_k^{(U)}/\tau_k^{(\Gamma)}$ approaches unity with increasing $\hat{k}$, signifying that the memory effect persists for relatively long times at short length scales. Meanwhile, $\tilde{\gamma}_k \tau_k^{(\Gamma)}$ approaches $\tau_k^{(\Gamma)}$ at large $\hat{k}$, implying that the duration of the early stage is shorter at small length scales. Therefore, dual relaxation clearly appears in SMT at intermediate length scales, where $\tau_k^{(\Gamma)}$ is not too short compared with $\tau_k^{(U)}$ and the friction coefficient due to TFs is much larger than the bare friction, i.e., $\tilde{\gamma}_k \ll 1$.

Mori and Okamura have proposed the affinity hypothesis between the correlation and memory functions [3], in which the correlation and memory functions have the same form of decay with different magnitudes and characteristic time scales.

FIG. 7. (Color online) Wave-number dependencies of the time scale $\tau_k^{(\Gamma)}$ for several values of : $\varepsilon = 0.050$ (purple), 0.20 (green), and 0.40 (red). Each dotted curve is obtained by a peak-fitting method and the vertical arrow points to where k_Γ is.
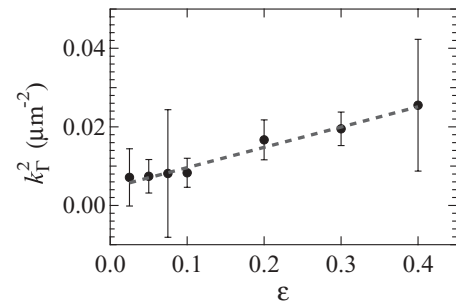

FIG. 8. ε dependence of k_Γ at which $\tau_k^{(\Gamma)}$ has a local maximum. The gray dashed line marks the line fit, $k_\Gamma^2 = c_0 + c_1\varepsilon$, with $c_0 = 0.0045$ and $c_1 = 0.052$. The exponent of the power law is suggested from the SMT patch structure: $\xi \sim \varepsilon^{-1/2}$.
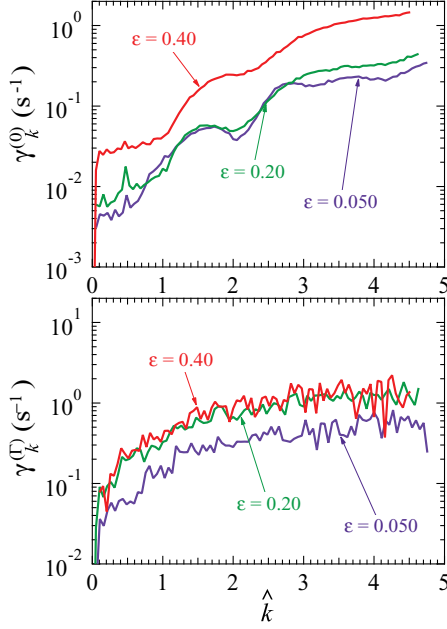
FIG. 9. (Color online) Dispersion relations for several ε values: $\varepsilon = 0.050$ (purple), 0.20 (green), and 0.40 (red). The top panel gives the bare-friction coefficient $\gamma_k^{(0)}$, and the bottom panel gives the friction $\gamma_k^{(\Gamma)}$ caused by TFs.

The main prediction from the hypothesis is that, when $\tau_k^{(U)}$ is almost the same as $\tau_k^{(\Gamma)}$, decay of the correlation features a long-time tail with exponent $-3/2$ over all spatial dimensions. Those time scales for SMT are almost the same for $\hat{k} \gtrsim 3.0$, as represented in Fig. 10. Our modal correlation functions in the long-time region however have a large margin of error; we cannot evaluate whether such long-time tails exist or not.

IV. CONCLUDING REMARKS

We experimentally observed the modal autocorrelation function $\hat{U}_k(t)$ of pattern dynamics in SMT. The modal relaxation dynamics featured a dual relaxation (Fig. 3); the correlation is well described by the time-reversible function at the early stage and by a simple exponential relaxation at the late stage. The corresponding time scales $\tau_k^{(a)}$ and $\tau_k^{(e)}$ obey dynamic scaling laws for the intrapatch scales (Fig. 4).

With an expectation that the patch structure generates memory effects due to the nonthermal fluctuations, we employed the projection-operator formalism in which the memory function naturally arises as the autocorrelation function of the nonthermal fluctuations. Indeed, we have verified the expectation; the peak wave number k_Γ (Fig. 8) of the time scale $\tau_k^{(\Gamma)}$ (Fig. 7) suggests that the dual relaxation is caused by intrapatch dynamics.

Solving the evolution equation [Eq. (7)] derived in the projection-operator formalism, we revealed two well-separated contributions for the nonthermal fluctuations in Fig. 5: rapidly varying Markovian fluctuations and non-Markov TFs. The former relates to the bare friction $\gamma_k^{(0)}$ and the latter to the memory function $\Gamma_k(t)$ [Eq. (9)]. SMT dynamics was shown analytically to separate into three stages (Table I): the bare-friction stage, $\tau \ll \tilde{\gamma}_k \tau_k^{(\Gamma)}$, where the relaxation is
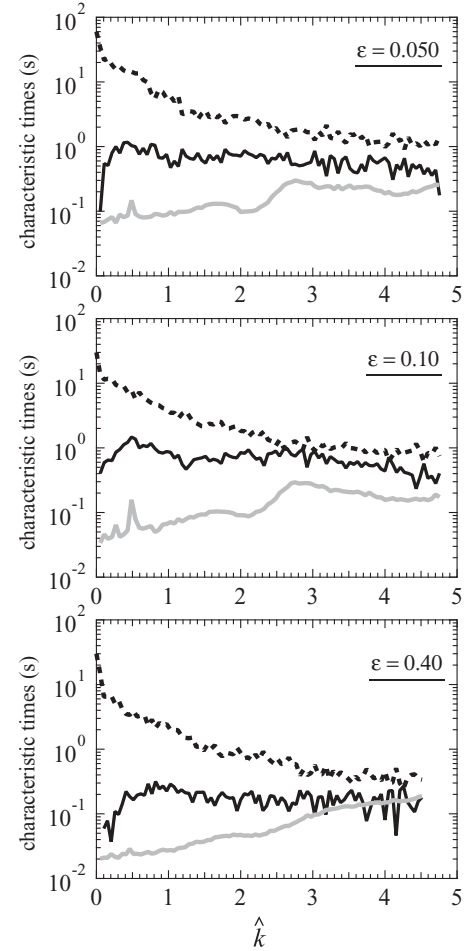

FIG. 10. Plot of the characteristic times $\tau_k^{(U)}$ (dashed line), $\tau_k^{(\Gamma)}$ (dark solid line), and $\tilde{\gamma}_k \tau_k^{(\Gamma)}$ (light solid line) for $\varepsilon = 0.050$ (top), 0.10 (middle), and 0.40 (bottom), respectively.

linear decay; the early stage, $\tilde{\gamma}_k \tau_k^{(\Gamma)} \ll \tau \ll \tau_k^{(\Gamma)}$, where the relaxation is time-reversible algebraic decay [Eq. (4)]; and the late stage, $\tau_k^{(\Gamma)} \ll \tau$, where the relaxation is simple exponential decay [Eq. (5)]. Further, by the variables defined in the theory (i.e., $\gamma_k^{(0)}$, $\gamma_k^{(\Gamma)}$, and $\tau_k^{(\Gamma)}$), we have analytically specified time scales obtained in experiments: $\tau_k^{(a)}$ [Eq. (17)], $\tau_k^{(e)}$ [Eq. (15)], and $\tau_k^{(U)}$ [Eq. (19)].

Comparison between the characteristic time scales (Fig. 10) clarified the nature of the dual structure in SMT. It clearly appears at intermediate length scales where the characteristic time $\tau_k^{(U)}$ of the modal relaxation is not too short compared with $\tau_k^{(\Gamma)}$ of the memory function due to TFs. Also, the friction coefficient $\gamma_k^{(\Gamma)}$ due to TFs is much larger than the bare friction $\gamma_k^{(0)}$.

The physical origin of the Markovian nonthermal fluctuations is still an open question. The dip near $\hat{k} \simeq 1$ in Fig. 9 suggests that the Markov contribution contains spatial features relating to electroconvection. That is, the bare friction consists of not only thermal fluctuations but also rapid variation in nonthermal ones. Note that the Markovian nonthermal fluctuations seem not to affect the SMT pattern dynamics, but act as a trigger for the onset of SMT. If nonthermal Markov fluctuations played a role in pattern dynamics, the modal

correlation would break time-reversal symmetry even at the early stage; nevertheless, early-stage relaxation is invariant under time reversal [Eq. (4)].

Besides SMT, several types of spatiotemporal chaos appear in the electroconvection of the liquid crystal systems. For example, instead of the homeotropic anchoring, one can apply the memory-function procedure to the planner anchoring as the boundary condition in which the rotational symmetry is not alive in the x-y plane. Our approach proposed in this paper can pave the way to understand them universally from the viewpoint of the nonthermal fluctuations relating to the pattern. This will be discussed elsewhere.

ACKNOWLEDGMENTS

APPENDIX: PROJECTION-OPERATOR FORMALISM

Physically, a macroscopic system can be divided into slowly varying behavior described by a set of macroscopic variables $\{A_i\}$ and rapidly varying terms [32,33]. The projection-operator formalism mathematically allows us to separate these two dynamics.

Using the linear projection operator, Mori mathematically derived a generalized linear Langevin equation containing a memory function [34]. The memory function is represented as a temporal correlation of the fluctuations $r_i(t)$, where $\langle r_i(t + \tau)A_j(t)\rangle = 0$. The generalized linear Langevin equation can be employed for not only equilibrium systems but also nonequilibrium systems. However, in the *linear* projection scheme, the fluctuation term $r_i(t)$ is orthogonal only to the linear functions of $\{A_i\}$ and can consist of not only the microscopic degrees of freedom but also fluctuations from nonlinear terms of $\{A_i\}$. Such *nonthermal* fluctuations are possibly relevant in nonequilibrium systems [35,36].

Zwanzig [37,38] formulated the generalized nonlinear Langevin equation by the *nonlinear* projection operator as

$$\dot{A}_i(t) = v_i(t) + J_i(t) + R_i^{(0)}(t), \tag{A1}$$

where $v_i(t)$ denotes the streaming term including nonlinear reversible terms and $J_i(t)$, an irreversible term. The fluctuation term $R_i^{(0)}(t)$ satisfies

$$\langle R_i^{(0)}(t + \tau)\mathcal{F}(A(t))\rangle = 0$$

for the arbitrary function $\mathcal{F}(A)$ of a set of macroscopic variables, $\{A_i\}$. The nonlinearity of $\{A_i\}$ is included in $v_i(t)$ and $J_i(t)$, and one can extract the linear part of $\{A_i\}$ from $v_i(t)$ and $J_i(t)$ using the *linear* projection-operator method. Mori and Fujisaka derived the evolution equation for the correlation function $U_{ij}(\tau) := \langle A_i(t + \tau)A_j^*(t)\rangle$ as [29,39]

$$\frac{\partial U_{ij}(\tau)}{\partial \tau} = \sum_l i\omega_{il}U_{lj}(\tau) - \sum_l \int_0^\tau d\tau' \Gamma'_{il}(\tau - \tau')U_{lj}(\tau'), \tag{A2}$$

where ω_{ij} denotes the mechanical coefficient and $\Gamma'_{il}(\tau)$ the memory function. Note that Eq. (A2), which relates the memory $\Gamma'(\tau)$ to the nonthermal fluctuations, is of the same form as the evolution equation derived in the linear projection-operator formalism; therefore, from a physical point of view, the obtained memory functions should be checked to see whether the memory effect originates from nonthermal fluctuations or not. If the characteristic time scale for the correlation of $R_i^{(0)}(t)$ is extremely short, then $R_i^{(0)}(t)$ satisfies

$$\langle R_i^{(0)}(t + \tau)R_j^{(0)}(t)\rangle \simeq 2\gamma_{ij}^{(0)}\delta(\tau), \tag{A3}$$

where $\gamma_{ij}^{(0)}$ denotes the bare-friction coefficient. In addition, if the fluctuations extracted from the nonlinear terms do not correlate with $R_i^{(0)}(t)$, the memory function due to the nonthermal fluctuations can be divided into two different terms,

$$\Gamma'_{ij}(\tau) = 2\gamma_{ij}^{(0)}\delta(\tau) + \Gamma_{ij}(\tau), \tag{A4}$$

where $\Gamma_{ij}(\tau)$ is regarded as the temporal correlation of the non-Markov contribution of the nonthermal fluctuations.

[1] S. Kai (ed.), *Pattern Formation in Complex Dissipative Systems: Fluid Patterns, Liquid Crystals, Chemical Reactions* (World Scientific, Singapore, 1991).

[2] M. Cross and P. Hohenberg, Rev. Mod. Phys. **65**, 851 (1993).

[3] H. Mori and M. Okamura, Phys. Rev. E **80**, 051124 (2009).

[4] V. Fréedericksz and V. Zolina, Trans. Faraday Soc. **29**, 919 (1933).

[5] A. Hertrich, W. Decker, W. Pesch, and L. Kramer, J. Phys. II (France) **2**, 1915 (1992).

[6] H. Richter, N. Klöpper, A. Hertrich, and A. Buka, Europhys. Lett. **30**, 37 (1995).

[7] M. I. Tribelsky and K. Tsuboi, Phys. Rev. Lett. **76**, 1631 (1996).

[8] S. Kai, K. Hayashi, and Y. Hidaka, J. Phys. Chem. **100**, 19007 (1996).

[9] Y. Hidaka, J.-H. Huh, K. I. Hayashi, S. Kai, and M. I. Tribelsky, Phys. Rev. E **56**, R6256 (1997).

[10] Y. Hidaka, J.-H. Huh, K. Hayashi, M. I. Tribelsky, and S. Kai, J. Phys. Soc. Jpn. **66**, 3329 (1997).

[11] F. Nugroho, T. Narumi, Y. Hidaka, J. Yoshitani, M. Suzuki, and S. Kai, Phys. Rev. E **85**, 030701(R) (2012).

[12] J.-P. Bouchaud, in *Anomalous Transport: Foundations and Applications*, edited by R. Klages, G. Radons, and I. M. Sokolov (Wiley-VCH, Weinheim, Germany, 2008), Chap. 11.

[13] H. Sillescu, J. Non-Cryst. Solids **243**, 81 (1999).

[14] M. D. Ediger, Annu. Rev. Phys. Chem. **51**, 88 (2000).

[15] R. Richert, J. Phys.: Condens. Matter **14**, R703 (2002).

[16] L. Berthier, G. Biroli, J.-P. Bouchaud, L. Cipeletti, and W. van Saarloos (eds.), *Dynamical Heterogeneities in Glasses, Colloids and Granular Materials* (Oxford University Press, Oxford, 2011).

[17] K. Tamura, Y. Hidaka, Y. Yusuf, and S. Kai, Physica A **306**, 157 (2002).

[18] Y. Hidaka, K. Tamura, and S. Kai, Prog. Theor. Phys. Suppl. **161**, 1 (2006).

[19] K. Tamura, R. Anugraha, R. Matsuo, Y. Hidaka, and S. Kai, J. Phys. Soc. Jpn. **75**, 63801 (2006).

[20] K. Tamura, Y. Yusuf, Y. Hidaka, and S. Kai, J. Phys. Soc. Jpn. **70**, 2805 (2001).

[21] R. Anugraha, K. Tamura, Y. Hidaka, N. Oikawa, and S. Kai, Phys. Rev. Lett. **100**, 164503 (2008).

[22] T. Nagaya, T. Takeda, and H. Orihara, J. Phys. Soc. Jpn. **68**, 3848 (1999).

[23] T. Nagaya and H. Orihara, J. Phys. Soc. Jpn. **69**, 3146 (2000).

[24] The *initial* and *final* regimes in Ref. [3] are respectively termed the *early* and *late* stages. As discussed in Sec. III B, SMT contains another stage that comes before the *initial* regime; therefore, for our study, the term *initial* is unsuitable.

[25] D. Forster, D. R. Nelson, and M. J. Stephen, Phys. Rev. A **16**, 732 (1977).

[26] V. Yakhot, Phys. Rev. A **24**, 642 (1981).

[27] M. Kardar, G. Parisi, and Y. C. Zhang, Phys. Rev. Lett. **56**, 889 (1986).

[28] Y. Hidaka, Y. Hosokawa, N. Oikawa, K. Tamura, R. Anugraha, and S. Kai, Physica D **239**, 735 (2010).

[29] H. Mori and H. Fujisaka, Phys. Rev. E **63**, 026302 (2001).

[30] There is no guarantee that a set of $\{u_k\}$ is complete in describing dominant dynamics. However, the fact remains that, to date, other slow variables have not been found in SMT; therefore, this assumption is not inconsequential.

[31] M. Suzuki, H. Sueto, Y. Hosokawa, T. Narumi, Y. Hidaka, and S. Kai (unpublished).

[32] M. S. Green, J. Chem. Phys. **20**, 1281 (1952).

[33] R. Kubo, Rep. Prog. Theor. Phys. **29**, 255 (1966).

[34] H. Mori, Prog. Theor. Phys. **33**, 423 (1965).

[35] K. Kawasaki, Ann. Phys. **61**, 1 (1970).

[36] R. Zwanzig, *Statistical Mechanics: New Concepts, New Problems, New Applications*, edited by S. A. Rice, K. F. Freed, and J. C. Light (University of Chicago Press, Chicago, 1972), pp. 241–256.

[37] R. Zwanzig, J. Chem. Phys. **33**, 1338 (1960).

[38] R. Zwanzig, Phys. Rev. **124**, 983 (1961).

[39] H. Mori and H. Fujisaka, Prog. Theor. Phys. **49**, 764 (1973).